Symposium on Thermoacoustics in Combustion: Industry meets Academia (SoTiC 2025)
Sept. 8 - Sept. 11, 2025
Trondheim, Norway
Paper No.: 77

The effect of transversal velocity fluctuations on the thermoacoustic response of reheat flames

Simon M. Heinzmann[1,2,†], Nino A. Leder[1,†] and Mirko R. Bothien[1,3]

Abstract

Thermoacoustic analysis remains a key component during the development process of new combustion chambers. Especially with the current challenges of creating fuel flexible combustion chambers, existing thermoacoustic models have to be improved and new ones created. There is a great deal of literature on the effect of longitudinal/planar acoustic waves on propagation-stabilized flames. Reheat flames only recently shifted into the scope of research, especially with regard to thermoacoustic modeling of the influence that transverse combustion chamber eigenmodes have on autoignition flames. In two previous publications, we showed how transverse eigenmodes influence the autoignition process. From this, the dynamic flame response was deduced, and stability predictions were made for two combustors and different operating points. In both studies, the assumption was made that transverse velocity perturbations have no effect on a one-dimensional autoignition flame. With the study presented here, we show the isolated effect of transversal velocity perturbations on the flame. This is done for two distinct flame stabilization cases occurring in a lab-scale reheat combustor. For the first, the flame is partly autoignition-stabilized but also has propagation-stabilized regions in the shear layer because of recirculation zones induced by a backward facing step. The second features only a minimal step height and therefore only minor recirculation zones, leading to an almost purely autoignition-stabilized flame. The two different flame stabilization cases are investigated using Reynolds-averaged Navier-Stokes simulations integrating an in-house reheat combustion model. The analysis shows that transverse velocity perturbations have no effect on flames that are purely stabilized by autoignition. In the presence of propagation-stabilized flame regions within the shear layer, transverse velocity perturbations do induce heat release rate fluctuations, as expected.

Keywords

thermoacoustic, autoignition, CFD, transverse eigenmodes, high-frequency

Novelty and Significance Statement

To date three approaches (1–3) exist to model the dynamic response of one-dimensional autoignition flames to longitudinal/planer acoustic waves. Recent studies (4; 5) showed for one of these models an adaption and integration in an FEM based framework to capture the thermoacoustic effects that the transverse acoustic eigenmodes of the combustion chamber have on non-compact autoignition flames. In this work, the dynamic heat release rate response of reheat flames perturbed by transversal velocity fluctuations was neglected. The presented paper aims to fill this gap by showing novel insights of how autoignition flames behave when perturbed by transversal velocity fluctuations. The significance of this work is twofold: firstly, it provides a more profound understanding on the influence that transverse eigenmodes have on autoignition flames. Secondly, it constitutes a valuable contribution to research in this field. These findings can support the industrial development of novel low-emissions gas turbine combustion chambers.

Nomenclature

Abbreviations

PV	Progress Variable
CFD	Computational Fluid Dynamics
FEM	Finite-Element-Method
FTF	Flame Transfer Function
HRR	Heat Release Rate
RANS	Reynolds Averaged Navier-Stokes

Greek

$\bar{\dot{\omega}}_{PV}$	Averaged turbulent source term of PV
$\dot{\omega}_{PV}$	Source term of PV
γ	Ratio of specific heats
Ω	Eigenfrequency
ω	Angular frequency in rad/s
ψ	Modeshape
ρ	Density

Roman

$(\cdot)'$	Perturbation in time domain
$(\cdot)_0$	Time-averaged quantity

[1]ZHAW Zurich University of Applied Sciences, Institute of Energy Systems and Fluid-Engineering, Winterthur, Switzerland
[2]ETH Zürich, Department of Mechanical and Process Engineering, Zürich
[3]Department of Energy and Process Engineering, NTNU, Norway
[†]These authors contributed equally to this work

Corresponding author:
S. M. Heinzmann, ZHAW Zurich University of Applied Sciences, Institute of Energy Systems and Fluid Engineering, Winterthur, Switzerland
Email: simon.heinzmann@zhaw.ch

$(\cdot)_{\text{init}}$	Initial
$(\cdot)_{eq}$	At equilibrium
$\hat{(\cdot)}$	Fourier transform of a fluctuating quantity
$\hat{\dot{q}}_{a,\psi_\Omega}(z)$	Fluctuating instantaneous HRR
c_0	Speed of sound
f_i	Mass fractions e.g. fuel, hot gas, carrier air
F_{ψ_Ω}	Modeshape dependent FTF
p	Pressure
$P(\cdot)$	Probability
p_{ref}	Pressure at reference location
T	Temperature
t	Time
T_i	Temperature of mass fraction i
x, y, z	x-,y- and z-coordinates
Y_i	Mass fraction of species i
$Y_{i,0}$	Initial mixture composition

Introduction

In order to comply with the Paris agreement (6), the future energy landscape must be based on renewable energy systems to ensure low emissions (7–9). Gas turbines firing alternative carbon-free fuels can be an ideal asset to balance and stabilize the power grid (8; 10–14). To fire a variety of fuels with very different combustion properties, extensive combustion chamber development is needed. When developing a new combustor, a critical challenge is a detailed thermoacoustic analysis to mitigate combustion instabilities (15). Thus, the need for more detailed and sophisticated thermoacoustic analysis tools is apparent.

The thermoacoustic analysis of longitudinal/planar acoustic waves on propagation stabilized flames has been extensively studied in the past (16–24). Nicoud et al. (16) showed how the thermoacoustic stability of combustion chambers with propagation-stabilized flames can be assessed using the finite element method (FEM) and a $n-\tau$ model, first introduced by Crocco (25). Schuermans (18) showed how the acoustics of complex geometries can be segmented into simpler subdomains described by a state-space representation and then concatenated in a network model to perform thermoacoustic analysis of acoustically compact flames with high accuracy. In the contrast to this, reheat flames only recently shifted into the scope of research (1; 3; 26–31). Bothien et al. (28) reconstructed the acoustic transfer matrix from a LES simulation of a backward-facing-step reheat combustor. Zellhuber et al (26), Gant et al. (1) and Gopalakrishnan et al. (3) derived frameworks to characterize the HRR response of 1D reheat flames perturbed by planar waves. Heinzmann et al. (4; 32) extended the numerical Lagrangian framework of Gopalakrishnan to compute modeshape dependent FTFs of transverse modes accurately.

In general, propagation-stabilized flames and autoignition flames react very differently to acoustic perturbations. However, the differentiation thereof is not trivial. Reheat flames in industrial gas turbine combustion chambers are usually composed of different heat release rate (HRR) regions. Certain regions of a reheat flame are solely stabilized by autoignition, others are stabilized by propagation. The propagation-stabilized HRR regions of reheat flames are typically located in the shear layers, which form due to recirculation zones at geometrical area jumps or around bluff bodies. The core of the reheat flame is autoignition stabilized within the bulk flow. The overall HRR distribution between the different zones is not fixed and can vary. With higher inlet temperatures in a sequential combustion chamber the overall HRR zone becomes more autoignition driven with characteristic shorter ignition delay times; and vice versa for colder conditions. While the propagation-stabilized HRR regions are governed by the balance of flame consumption speed and local flow velocity, the autoignition is governed by the balance between chemical and residence time scales. Acoustic fluctuations can have a large impact on both flame zones.

With respect to perturbations in transverse direction, transversal acoustic waves can significantly affect the flame shape and HRR. Close to geometric discontinuities, such as area jumps, transversal acoustic eigenmodes can induce vortex shedding and modulate the reactive shear layers. This leads to HRR fluctuations locally within the propagation-stabilized part of the flame (33). The autoignition-stabilized HRR regions are sensitive to acoustic pressure and isentropic temperature fluctuations, which modify the local ignition delay time and therefore shift the flame back and forth (3; 4). Heinzmann et al. (4; 5) developed a framework to model the dynamic effect that such modes have on reheat flames. They assessed transverse eigenmode stability and validated it with experiments. An assumption of the framework is, that transverse velocity perturbations have negligible effect on a one-dimensional (1D) autoignition flame. This assumption is based on the fact that reheat flames react significantly weaker to velocity fluctuations in flow direction when compared to temperature and pressure fluctuations. This can be seen by the low value of the FTF with respect to velocity perturbations in Ref. (28). The mechanism responsible for the HRR response due to in flow oriented velocity perturbation is the modulation of the equivalence ratio (1; 2; 26; 34). However, no equivalence ratio fluctuations are present in the case of transverse velocity perturbations in fully premixed conditions. A homogeneous premixed mixture upon entry into the combustion chamber was confirmed by a prior study for the investigated combustor (35). In-house CFD simulations also concluded a good mixing of fuel and air before entering the combustor. Thus, the modeshape-dependent FTF $F_{\psi_\Omega}(\omega)$ for a certain eigenmode Ω to compute the fluctuating instantaneous heat release rate (HRR) $\hat{\dot{q}}_{a,\psi_\Omega}$ of Eq. 1 is assumed to remain unaffected by transverse velocity perturbations (4).

$$\hat{\dot{q}}_{a,\psi_\Omega}(z) = \dot{q}_{0,a}(z) F_{\psi_\Omega}(\omega) \frac{\hat{p}(x_{ref}, z)}{p_0} \tag{1}$$

To the best of our knowledge, there is no literature to date stating whether transverse velocity perturbations have an effect on 1D reheat flames. In this paper, we identify the dynamic HRR response for two distinct cross-sections of a rectangular lab-scale reheat combustion chamber (36). This is done by acoustically exciting the first transverse modes for both dimensions of a rectangular combustion chamber (i.e. in xy- and xz-direction) in unsteady compressible RANS

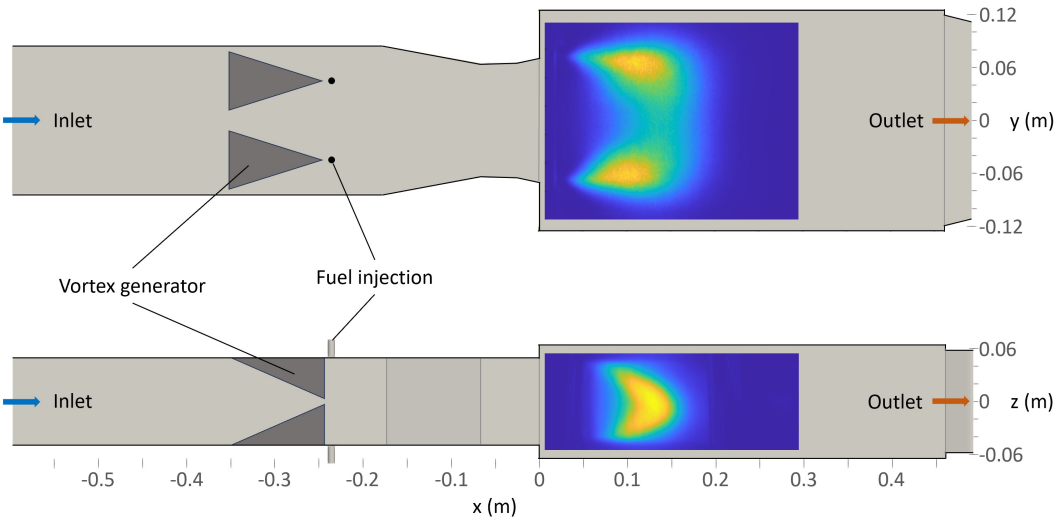

Figure 1. Geometry of the reheat combustion chamber at TUM. The xy-cross-section is shown on the top, and the xz-cross-section on the bottom. Qualitative experimental flame images are shown solely for the visualization purpose (different operating point).

simulations. To identify and isolate whether transverse velocity fluctuations have negligible effect on a pure reheat flame, two different simulations are performed for each of the dimensions (four in total). Non-compact Fourier decomposition is done of the results to identify the flame response of both the autoignition stabilized flame parts as well as the propagation-stabilized assisted flame regions.

Methodology

The methodology section describes how the RANS computation is setup. First, the geometry is shown. Second, the combustion model is introduced. Third, the numerical setup is discussed. Fourth, the mean fields are shown and lastly, the implementation of the transverse forcing is discussed.

Combustor geometry

The atmospheric combustor of the Technical University of Munich (TUM) (36) shown in Fig. 1 consists of a vitiator followed by a reheat combustor. The vitiator is operated with a lean, perfectly premixed, preheated and with a mixture of hydrogen and methane. The vitiated air enters the reheat combustor and passes through a mixing section where the fuel is injected into the hot gas in a jet-in-cross-flow arrangement. To improve mixing, delta wing-shaped vortex generators are placed upstream of the fuel injection. The mixture then passes through a convergent section before entering the reheat combustion chamber through a diffuser-shaped outlet. The rectangular combustion chamber mainly expands in y-direction, which leads to strong upper and lower recirculation zones downstream of the area jump. In z-direction, the combustion chamber does not expand significantly, and thus no significant recirculation zones are observed. For more details on the sequential combustor, the reader is referred to Refs. (4; 33; 36; 37).

RANS computation

The RANS CFD computations are performed for the presented rectangular reheat combustion chamber (Fig. 1) burning a mixture of 50% methane and 50% hydrogen by weight at lean and autoignitive conditions. The CFD is done using ANSYS Fluent 2024 R1 (38) using the realizable $k-\epsilon$ model for turbulence with an adaptive Schmidt number to obtain better mixing results at the jet-in-crossflow fuel injection. A RANS version of the combustion model derived by Kulkarni et al. (39; 40) was implemented and extended to capture the effects of acoustic waves.

This combustion model is based on a transported normalized progress variable (PV) which represents intermediate species reactions that govern the ignition delay. In contrary to using a linear PV, reaction species from the radicals (CH_2O, CO, HO_2) and product pool (CO_2, H_2O) are used to properly capture the ignition process. The advantage of including the (hot) products is that the propagation-stabilized flames in the shear layer of the recirculation zones are captured more accurately. The normalized PV is obtained by dividing the sum of the included species mass fractions by its sum at equilibrium:

$$PV = \frac{\sum Y_i}{\sum Y_{i,\mathrm{eq}}} \tag{2}$$

The PV source term can be computed using finite differencing. For the model to work, the source term must be strictly positive and only depend on known parameters like the local fuel mass fraction f_F, hot gas mass fraction f_H, temperature, pressure and the value of the PV itself. By splitting the temperature and pressure into its mean and fluctuating part, and under the assumption that the mean value of the temperature and pressure are constant during the radical buildup, the PV source can be expressed as:

$$\dot{\omega}_{PV} = \dot{\omega}_{PV}\left(f_i, T_{0,\mathrm{init}}, T', p_0, p', PV\right) \tag{3}$$

In their combustion models, Brandt (41) and Kulkarni (39) assumed that the transport of energy scales the same as

the transport of mass, and that the change of specific heat capacity c_p upstream of the flame is negligible. Therefore, the initial temperature can be expressed through the mass fractions f_i and the known initial temperatures $T_{i,\text{init}}$:

$$T_{0,\text{init}} = \sum T_{i,\text{init}}\, f_i \tag{4}$$

Assuming an isentropic correlation of pressure and temperature for acoustic waves, T' can be expressed through p', and as the operating pressure p_0 is known, the PV source can be simplified to:

$$\dot{\omega}_{PV} = \dot{\omega}_{PV}\left(f_i, p', PV\right) \tag{5}$$

To model the Turbulence Chemistry Interaction (TCI) a PDF approach for the mass fractions f_i and the PV is used. The mean turbulent source term is obtained by folding the sources over a probability distribution:

$$\overline{\dot{\omega}}_{PV} = \int_0^1 \left(\int_0^1 \dot{\omega}_{PV}(f_i, p', PV)\, P(f_i)\, df_i \right) P(PV)\, dPV \tag{6}$$

The HRR is then obtained by using the mixed is burned approximation and delaying it by multiplying the reaction rate with the PV.

The major advantage of this approach is that it is computationally cheap. The source terms, which can be computed using 0D reactors, and the integration can be done *a priori* and stored. Therefore, only the educts, products, PV, its variance and the mass fractions with their variances need to be transported, and no expensive reaction rate computations are necessary. Using this approach, it is assumed that there is no interaction between the individual reactors during computations. Performing 0D reactor mixing studies, Brandt (41) verified this assumption and obtained an overall error below 10%.

In this paper, the PV source terms were computed using the GRI30 (42) mechanism and the probability distributions for integration were created using modified curl mixing of particles (43). To reduce PV source lookup time during the simulation, a Residual Network is used to retrieve the sources. Residual Networks are neural networks where each block adds a skip connection. The skip connection helps with the training stability and accuracy for deeper networks by mitigating vanishing gradients and overfitting. The network used here consists of an input block followed by three residual blocks, each consisting of two fully connected layers with a skip connection, and an output layer (44).

First transverse eigenmode	Simulation nomenclature	
	all effects	without p' and T' effects
y-direction	T1y	T1yNPE
z-direction	T1z	T1zNPE

Table 1. Simulation nomenclature depending on eigenmode and accounted HRR effects.

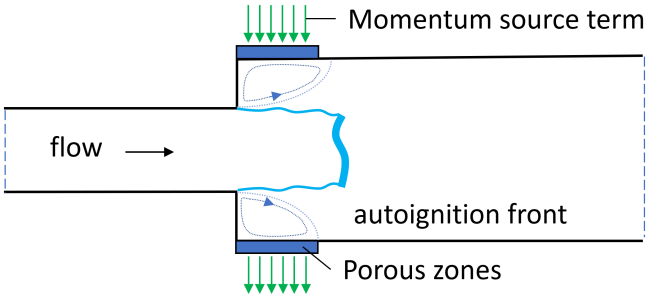

Figure 2. Porous zones and momentum source terms.

Property	**Hot Gas**	**Fuel premixed with additional air**
$\dot{m}$ [g/s]	366.46	8.55
T [K]	967	283.15
Y_{O_2}	0.168	0.123
Y_{N_2}	0.76	0.461
Y_{CO_2}	0.039	-
Y_{H_2O}	0.032	-
Y_{CH_4}	-	0.208
Y_{H_2}	-	0.208

Table 2. Gas properties

Four simulations are computed in total. Table 1 displays the naming convention, depending on the orientation of the first eigenmode as well as the HRR effects accounted for. The T1y- and T1z-simulations are computed for the first transverse eigenmode in y- and z-direction (Fig. 1), respectively, with the inclusion of local acoustic pressure and temperature fluctuations effects. The T1yNPE- and T1zNPE-simulations (NPE: No Pressure Effects) do not account for a change in HRR due to local pressure and temperature fluctuations in the CFD progress variable. Thus, the flame only reacts to velocity and equivalence ratio fluctuations. For the NPE cases, p' is set to zero for the source term lookup. Therefore, the effect of the pressure and temperature change induced by acoustic waves is ignored during the simulation.

The computational domain (Fig. 3) is half of the reheat combustor (36) making use of the symmetry planes xz and xy for efficiency. The mesh is made up of approximately $1.3{*}10^6$ cells with refinements at the walls, the area changes and the fuel injection. A mesh independence study comparing the fuel mixture fractions at the dump plane as well as the magnitude and position of the HR shows no variation for a finer mesh. Time and space are discretized in second order and the timestep is set to 4e-7s to obtain an acoustic CFL below one. The operating point, which is shown in Tab. 2, is equal to the NG_{50med} operating point from Franke et al. (36).

The excitation is achieved in a similar way as was shown by Zellhuber et al. (45). On the combustor walls, which coincide with the antinodes of the first transversal eigenmode, small porous zones with high resistance are added, Fig. 2 and Fig. 3. Within these zones, momentum source terms are applied to force of the fluid domain. The precise forcing frequencies of the T1y-and T1z modes are calculated by solving the homogeneous Helmholtz equation Eq. 7 in COMSOL 6.2.

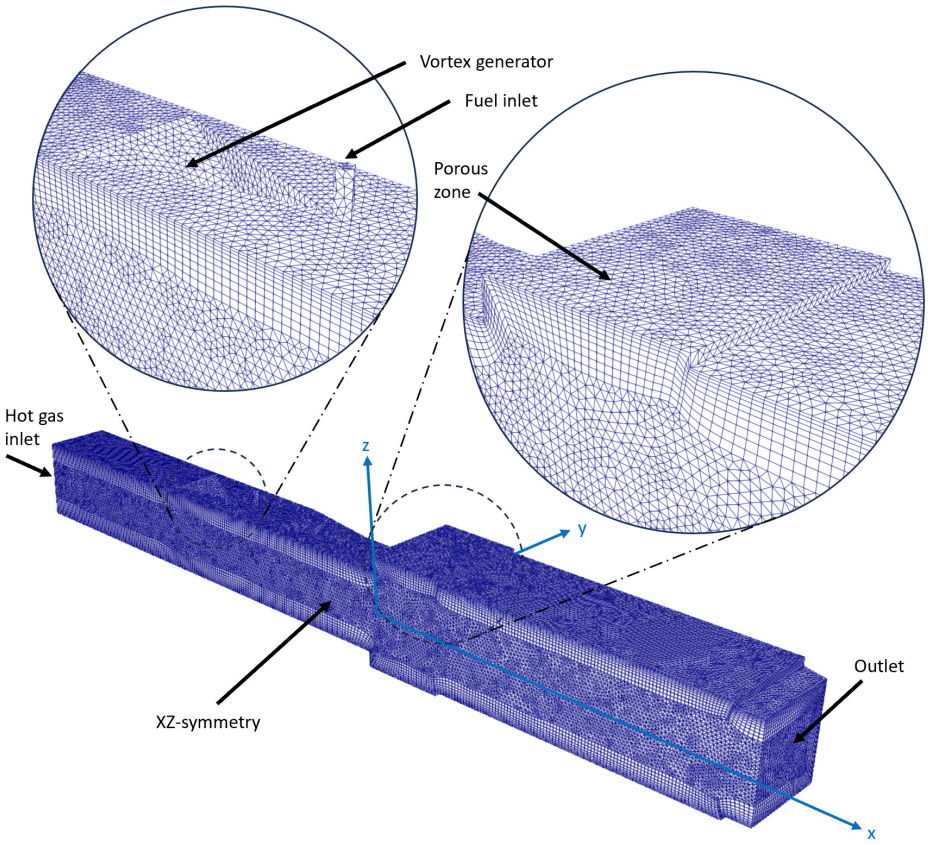

Figure 3. Half of the CFD mesh and computational domain.

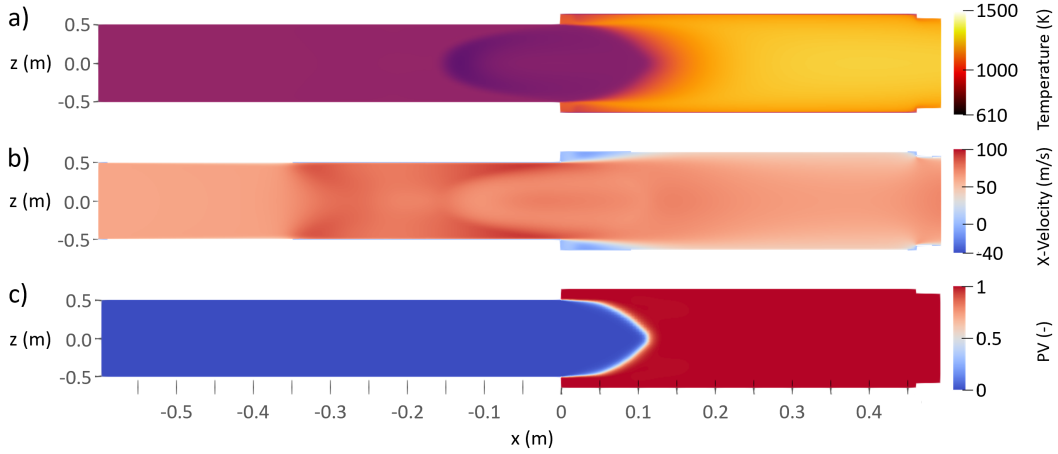

Figure 4. CFD mean fields for the xz-cross-section: a) temperature field, b) x-velocity field and c) progress variable (PV).

$$\nabla \cdot \left(\frac{1}{\rho_0} \nabla \hat{p} \right) + \frac{\omega^2}{\gamma p_0} \hat{p} = 0 \tag{7}$$

The time averaged flame is accounted for in the FEM study by inclusion of the time averaged temperature field in the combustion chamber, which is taken from the steady CFD computation.

Results

First the CFD mean field results are shown and the time averaged HRR field is validated for the xy-cross-section using experimental data from (36). Subsequently, observations are made for two distinct geometrical planes of the combustion chamber. Then, the xy-plane ($z = 0$) is analyzed where the flame response is composed of autoignition and propagation-stabilized flame regions for both the T1y and T1yNPE simulations. The subsequent section presents the results of the analysis of the xz-plane ($y = 0$). Here, the flame is predominantly autoignition stabilized (4; 29), and comparisons are drawn between the T1z- and T1zNPE simulations.

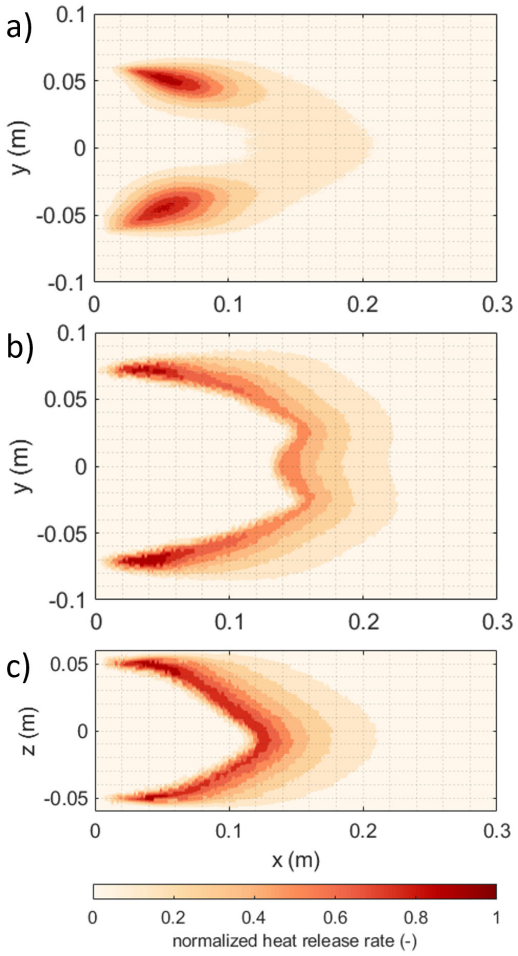

Figure 5. a) Time averaged HRR mean field on the xy-plane of the experimental line-of-sight-integrated chemiluminescence imaging (36), b) time averaged HRR mean field on the xy-plane of the RANS computation, c) the time averaged HRR mean field on the xz-plane of the RANS computation.

CFD steady HRR mean field validation

Fig. 4 shows the temperature, x-velocity and PV contours from the RANS computation for the xz-cross-section. Fig. 4a) shows a uniform temperature distribution at the inlet of the combustion chamber. Fig. 4b) indicates that the recirculation zones induced by the step are small. Fig. 4c) shows the result of the in-house combustion model. The earlier timed ignition at the corner of the area jump is captured because of the inclusion of (recirculating) hot products. On the x-axis the flame is purely autoignition-driven and the position matches with the analytical mean ignition delay time also reported in Ref. (36).

The time averaged flow field and flame shape of the CFD simulation is validated using experimental data (36). Fig. 5 shows the average HRR on the xy-plane for a) the chemiluminescence measurement and b) the CFD simulation. The mean ignition length (i.e. ignition delay time) is computed by assessing Gaussian kernel fits of the HRR in x-direction. The value of 0.16m from the dump plane matches very well for the central cross-section (y = 0). This indicates that the implemented in-house combustion model is able to accurately predict the flame's average location. Toward the combustor walls, the flame is located further upstream as a result of the lower axial velocity due to the recirculation zones after the area jump at the dump plane. The implemented reheat model is able to capture the shear-layer flames. The RANS computation predicts the strongest zones of the shear layer flames slightly further upstream, which is believed to be a numerical artifact of the solver. In addition, the center of the flame that is solely autoignition stabilized is pronounced more strongly in the CFD compared to the experiment. This could be due to multiple reasons. A main factor could be that in the CFD simulation the mixture enters the dump plane with a uniformly spread fuel mixture fraction. The homogeneity of this parameter is affected by the induced vortical structures of the vortex generators ahead of the fuel injectors. Thus, there could be slight differences in the modeling of these effects in relation to the experiment. Also, the jet-in cross-flow fuel injection momentum could be slightly different in the experiment compared to the simulation. A lower momentum of the fuel jet could lead to smaller fuel mass fractions towards the center of the combustor. However, the time-averaged HRR mean field of the CFD can capture the structure of the experimentally measured HRR mean field. With respect to the xz-plane (Fig. 5c), there are no experimental measurements to validate the mean field. However, the identical combustion chamber was used in (46), where a similar flame shape was determined for a different operating point burning methane and propane. Also, for this cross section, it is believed that the HRR close to the walls is too far upstream in the RANS computation due to the solver. Still, the CFD mean field is accurate and can be used for the targeted study to identify the effect that transverse velocity perturbations have on a reheat flame.

The excitation frequencies were determined by solving Eq. 7 in FEM, analogously to (4). The effect of the flame is accounted for by including the time-averaged temperature field in the combustion chamber. For the T1y-mode the forcing frequency is 1426Hz and for the T1z-mode 2660Hz. Fig. 6a) shows the first transverse eigenmode of the xz-plane obtained by the eigenfrequency study using FEM. Fig. 6b) shows the instantaneous pressure perturbations of the excited first transverse mode at an identical frequency of 2660Hz. The comparison shows an excellent match between the modeshapes. The same is the case for the T1y mode (not shown). Thus, it is confirmed that the first transverse eigenmodes are correctly excited in the CFD simulation.

Propagation-and autoignition stabilized flame regions on the xy-plane

Analyzing the flame response on the xy-plane, distinct observations can be made. Fig. 7a) shows the pressure perturbations in the first column, the transverse velocity perturbations in the second column, and the HRR perturbations in the third column for the T1y-simulation. All quantities are plotted for half and oscillation from 90° to 270°. It is visible that the first transverse acoustic mode has an effect on the partly autoignition-stabilized reheat flame. An alternating HRR perturbation pattern is clearly visible at a phase of 180°. At this phase, the upper ($y > 0$) HRR perturbation in the shear layer flame is around 180° out of phase with the transverse velocity perturbation. The lower

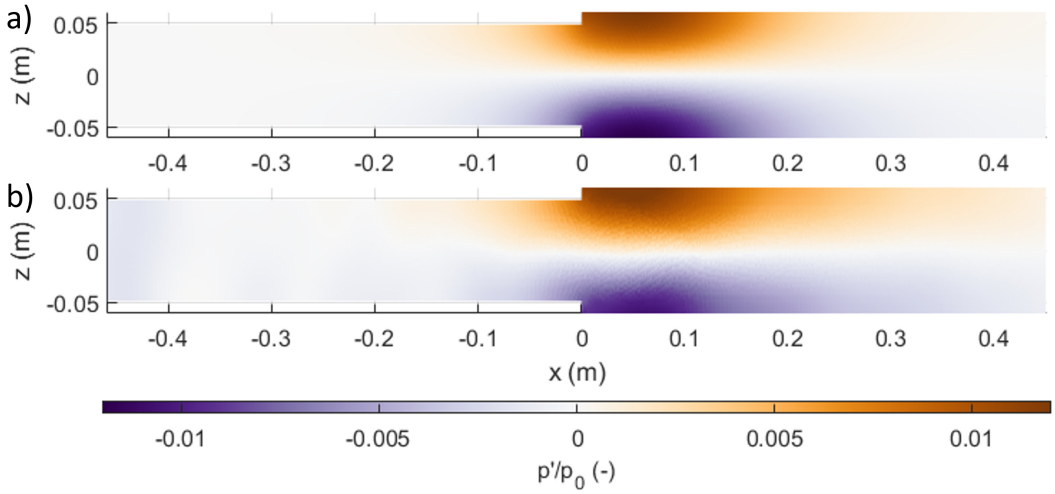

Figure 6. a) T1z acoustic eigenmode of the FEM computation, b) T1z acoustic eigenmode of the RANS computation.

($y < 0$) HRR perturbation in the shear layer flame is in phase with the velocity perturbation. The same behavior is not observed for the T1yNPE-simulation shown in Fig. 7b). Therefore, the clearly observable HRR perturbation pattern in the T1y-simulation is believed to occur due to pressure and temperature effects. The very local and small HRR fluctuations right after the dump plane ($x = 0$) are very similar in both simulations, and no qualitative differences are observed. Most likely, they are induced by vortical structures that originate right after the dump plane. This behavior was also observed in prior experiments of the experimental setup by McClure et al. (33). The tracking of more/less intense HRR perturbation patches revealed that these vortical structures are transported with the mean flow (33). They are contained between the shear layers of the recirculation zones, i.e. in the propagation-stabilized shear layer flames. With respect to the central symmetry line ($y = 0$), no HRR fluctuations are present in both simulations. This is interesting to observe, because the central symmetry line is a nodal line of the pressure modeshape and an antinode for the velocity perturbations. Thus, on this line, a fluid particle experiences no pressure fluctuation, but indeed the strongest velocity fluctuations. Therefore, it is found, that the transverse velocity fluctuations have no influence on a solely autoignition stabilized reheat flame segment at ($y = 0$). This is further supported by the experimental results from McClure et al. (33) for the same combustion chamber. In the experiment, the identical first transverse mode was measured in the combustor and no flame modulation was found of the autoignition core region.

Quantitative comparisons between the simulations can also be made. By integrating the HRR for multiple cross-sections parallel to the x-axis and relating the integral quantity to the local velocity perturbations slightly upstream of the flame front, specific local FTFs can be computed. Fig. 8 shows the local FTFs for a) the T1y-simulation and b) the T1yNPE-simulation. The integrated HRR is plotted by the dashed black line to identify which locations correspond to the more strongly pronounced shear layer flames. The following observations are made:

- The transverse velocity fluctuations induce no HRR fluctuation for the center cross-section ($y = 0$), which is visible by the gain of 0. This is the case for both simulations (Fig. 8a)) and Fig. 8b). This is particularly meaningful, as this cross-section at ($y = 0$) coincides with the antinode of the transverse velocity perturbation field. Thus, if the transverse velocity had an effect on a reheat flame, it would appear the strongest for this cross-section. Thus, the initial hypothesis that a transverse velocity does not affect the HRR response of a solely autoignition stabilized flame is confirmed.
- The phase of the T1y-HRR response in the shear layer flames oscillates around 0 for the flame located on the negative y-axis, and $-\pi/2$ for the flame located on the positive y-axis. Whilst the velocity perturbation has the same phase on the investigated plane, the pressure and resulting isentropic temperature perturbations are out of phase towards the combustor walls (antinodes are at the walls). This is most-likely the reason for the different phase in the HRR-response compared to the T1yNPE-simulation. For the T1yNPE-simulation, the phases of the HRR-response of the shear layer flames appear similar at around $-\pi/2$.
- The peaks in the FTF gain coincide with the stronger shear layer HRR flame regions.
- The gain of the HRR-response of the shear layer flames is significantly higher in the T1y-simulation compared to the T1yNPE-simulation. This is due to the fact that no HRR-response due to pressure and isentropic temperature perturbations is accounted for in the latter. Further, the shear layer flames are located closely to the pressure antinodes, which suggests a pronounced HRR-response.
- Towards the combustor walls, the transverse velocity field has its antinodes. Hence, as the y-coordinate approaches the location of the combustor walls, the transverse velocity measures low values which can result in a high sensitivity of the computed FTF.

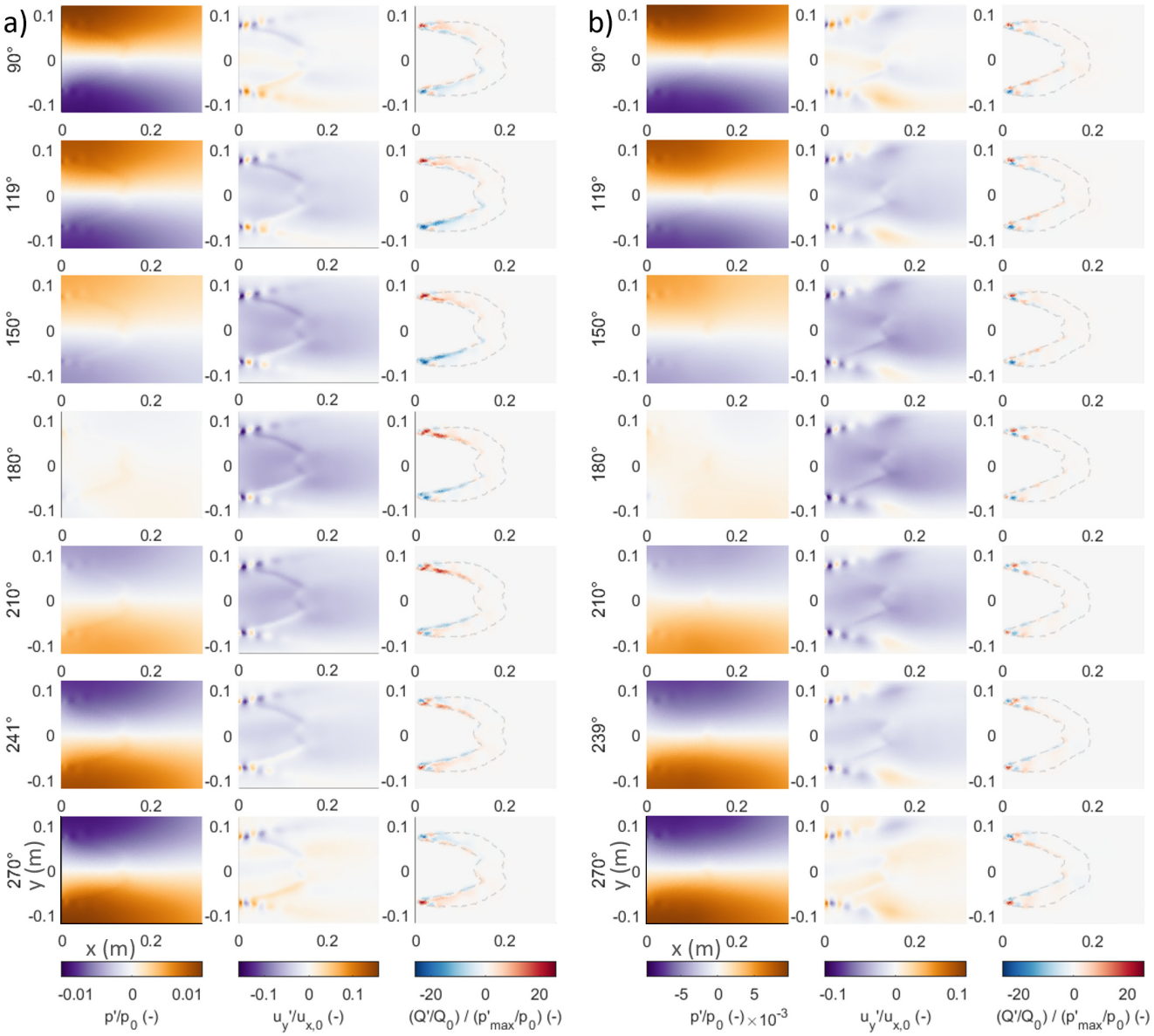

Figure 7. a) Pressure perturbations (first column), transverse velocity perturbations (second column), and HRR perturbations (third column) for the T1y-simulation and half an oscillation. The same variables are plotted in b) for the T1yNPE-simulation.

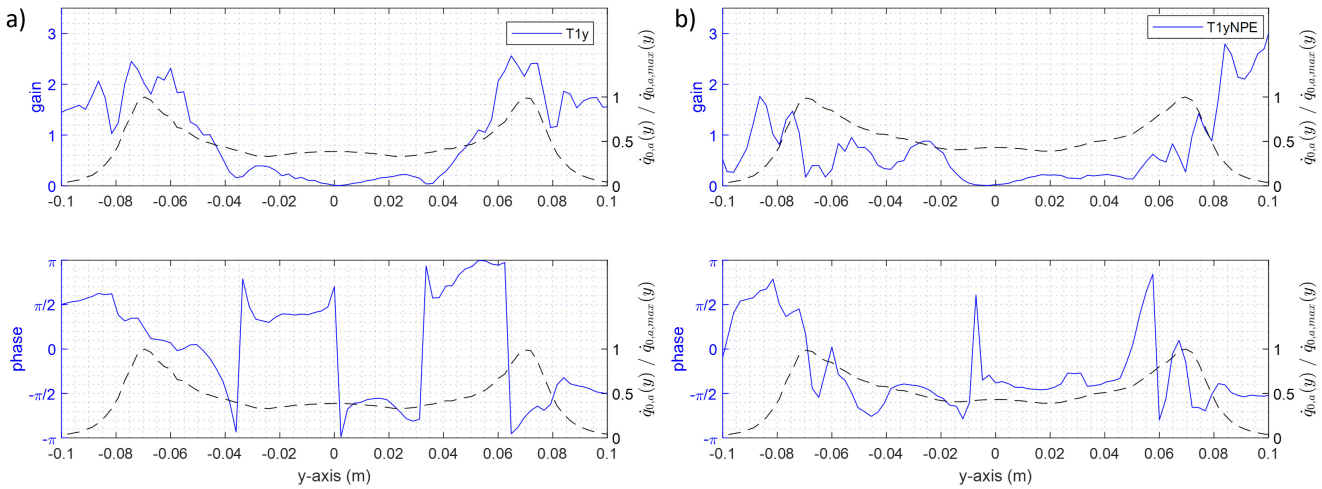

Figure 8. The local FTFs to velocity fluctuations for a) the T1y-simulation and b) the T1yNPE-simulation. The integrated HRR is plotted by the dashed black line.

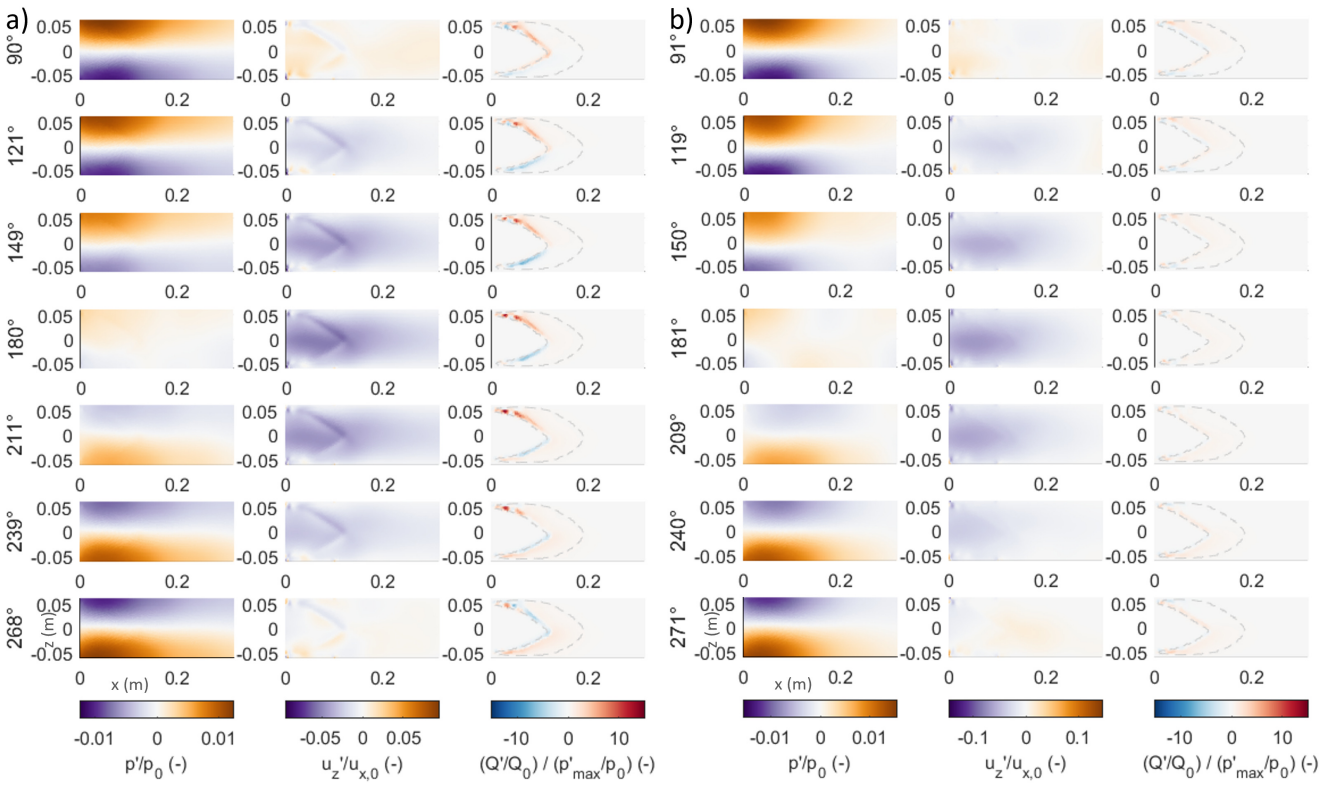

Figure 9. a) Pressure perturbations (first column), transverse velocity perturbations (second column), and HRR perturbations (third column) for the T1z-simulation and half an oscillation. The same variables are plotted in b) for the T1zNPE-simulation.

Autoignition stabilized flame regions on the xz-plane

Similar comparisons as for the xy-plane can be made for the xz-plane. The main difference between the cross-sections is, that the xz-HRR field is predominantly stabilized by autoignition. The minimal area jump at the dump plane induces smaller recirculation zones. Therefore, only a small portion of the flame is propagation stabilized in the shear layer. Fig. 9a) shows the same quantities plotted as in Fig. 7a) for the xz-plane and the T1z-simulation. A very distinct pattern of the HRR-response on the upper and lower flame regions are observed. The HRR perturbations intensify towards the outer combustor walls and are out of phase with the transverse velocity for the upper flame regions and in phase for the lower flame regions. The HRR fluctuation pattern looks very similar to the numerical computations and the experimental data in (4). In contrast, the T1zNPE-simulation does not reproduce the same HRR-response. Without inclusion of the pressure and isentropic temperature effects on the flame, the HRR-response is near 0 for most of the flame region. This is to be expected, as the analysis for the xy-plane already showed no effect of the transverse velocity on the central cross-section. Hence, it is also confirmed for the xz-plane that the transverse velocity fluctuations have no effect on the HRR of the flame. The experimental data shown in (4) for the same cross-section further supports this.

The local FTFs of the integrated HRR (integrated along the x-axis) and the velocity perturbation upstream of the flame are shown in Fig. 10a) for the T1z-simulation, and in Fig. 10b) for the T1zNPE-simulation. In a) it is clearly observable that the central cross-section at $z = 0$ has a gain close to zero, meaning that the flame response is negligible. The same observation is made for the T1zNPE-simulation. The small gain of 0.07 for $z = 0$ of the T1zNPE-simulation arises from a slight decrease of the T1z modeshape amplitude over one harmonic cycle. As a result, the HRR of the first 50% of the cycle does not average to zero with the second 50% of the cycle, as is the case for the other simulations. For the T1zNPE simulation, obtaining a close to constant modeshape amplitude for multiple cycles remained more challenging compared to the other simulations. Nonetheless, the negligible gain can be attributed to these numerical difficulties, and the results support the same findings from the other simulations. Therefore, the initial hypothesis of Heinzmann et al. (4; 32), that transverse velocity perturbations have no effect on a solely autoignition stabilized flame, is confirmed.

Conclusion

The effect of transverse acoustic eigenmodes on autoignition flames has been investigated in recent studies (4; 32). In this paper, we specifically further analyze the effect that transversal velocity fluctuations have on fully- and partly-autoignition-stabilized flames. For this, unsteady forced RANS computations are performed in Fluent of a lab-scale reheat combustor (29) and the mean fields validated with experimental measurements. The analysis shows that transverse velocity perturbations have no effects on flames solely stabilized by autoignition. This was confirmed in all four simulations. Therefore, the initially stated hypothesis is confirmed. For partly autoignition stabilized flames, where

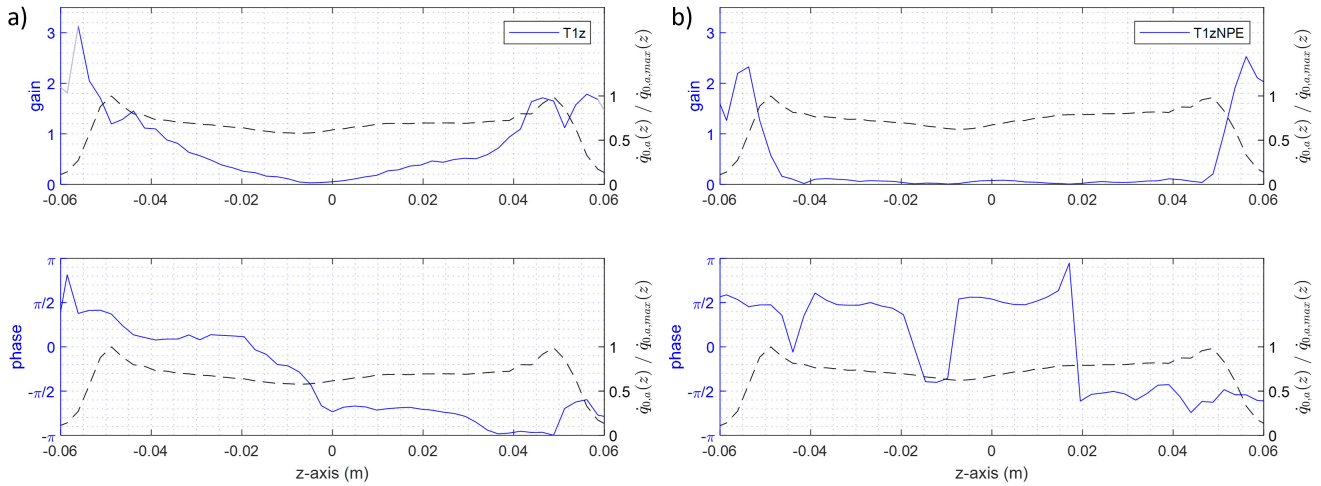

Figure 10. The local FTFs to velocity fluctuations for a) the T1z-simulation and b) the T1zNPE-simulation. The integrated HRR is plotted by the dashed black line.

propagation-stabilized parts are present in the shear layer, transverse velocities can have an effect. Still, the local effects of pressure and isentropic temperature tend to have a significantly stronger effect compared to the transverse velocity.

Acknowledgements

The research work presented in this manuscript was carried out within the FLEX4H2 project. The FLEX4H2 project is supported by the Clean Hydrogen Partnership and its members European Union, Hydrogen Europe and Hydrogen Europe Research (GA 101101427), and the Swiss Federal Department of Economic Affairs, Education and Research, State Secretariat for Education, Research and Innovation (SERI). Views and opinions expressed are however those of the author(s) only and do not necessarily reflect those of the European Union or any other granting authority. Neither of them is liable for any use that may be made of the information contained therein.

References

[1] Gant F, Gruber A and Bothien MR. Development and validation study of a 1D analytical model for the response of reheat flames to entropy waves. *Combustion and Flame* 2020; 222: 305–316. DOI:10.1016/j.combustflame.2020.09.005.

[2] Zellhuber M, Schuermans B and Polifke W. Impact of acoustic pressure on autoignition and heat release. *Combustion Theory and Modelling* 2014; 18: 1–31. DOI: 10.1080/13647830.2013.817609.

[3] Gopalakrishnan HS, Gruber A and Moeck J. Response of auto-ignition-stabilized flames to one-dimensional disturbances: Intrinsic response. *J Eng Gas Turbines Power* 2021; 143: 121011. DOI:10.1115/1.4052058.

[4] Heinzmann SM, Gopalakrishnan HS, Gant F et al. Development and validation of a framework to predict the linear stability of transverse thermoacoustic modes of a reheat combustor. *Combustion and Flame* 2025; 275: 114010. DOI:https://doi.org/10.1016/j.combustflame.2025.114010. URL `https://www.sciencedirect.com/science/article/pii/S0010218025000483`.

[5] Heinzmann SM, Gopalakrishnan HS, Wood B et al. Linear stability analysis of transversal thermoacoustic modes in reheat combustors. *Proceedings of GT2025 ASME Turbo Expo 2025,GT2025-152879, accepted* 2025; .

[6] United Nations. Paris agreement, 2015.

[7] IEA. World energy outlook 2022, 2022.

[8] Bundesamt für Energie. Energieperspektiven 2050+, 2021.

[9] Expert Group Security of Supply ETH Zurich. Energy security in a net zero emissions future for switzerland, 2023.

[10] Ciani A, Bothien M, Bunkute B et al. Superior fuel and operational flexibility of sequential combustion in Ansaldo Energia gas turbines. *J Glob Power Propuls Soc* 2019; 3: 630–638. DOI:10.33737/jgpps/110717.

[11] Bothien MR, Ciani A, Wood JP et al. Toward decarbonized power generation with gas turbines by using sequential combustion for burning hydrogen. *J Eng Gas Turbines Power* 2019; 141: 121013. DOI:10.1115/1.4045256.

[12] Farhat H and Salvini C. Novel gas turbine challenges to support the clean energy transition. *Energies* 2022; 15. DOI: 10.3390/en15155474.

[13] Goldmeer J, Buck C, Suleiman B et al. Techno-economic analysis of hydrogen and ammonia as low carbon fuels for power generation. In *Proceedings of ASME Turbo Expo 2023*.

[14] Kloess M and Zach K. Bulk electricity storage technologies for load-leveling operation - an economic assessment for the austrian and german power market. *International Journal of Electrical Power and Energy Systems* 2014; 59: 111–122. DOI:10.1016/j.ijepes.2014.02.002.

[15] Bothien MR, Pennell DA, Zajadatz M et al. On key features of the aev burner engine implementation for operational flexibility. Proceedings of ASME Turbo Expo 2013.

[16] Nicoud F, Benoit L, Sensiau C et al. Acoustic modes in combustors with complex impedances and multidimensional active flames. *AIAA Journal* 2007; 45: 426–441. DOI: 10.2514/1.24933.

[17] Campa G and Camporeale S. Eigenmode analysis of the thermoacoustic combustion instabilities using a hybrid technique based on the finite element method and the transfer matrix method. *ADVANCES IN APPLIED ACOUSTICS* 2012; 1: 1–14.

[18] Schuermans B. *Modeling and control of thermoacoustic instabilities*. PhD Thesis, EPFL, 2003.

[19] Schuermans B, Bellucci V, Guethe F et al. A detailed analysis of thermoacoustic interaction mechanisms in a turbulent premixed flame. In *Proceedings of ASME Turbo Expo 2004 Power for Land, Sea, and Air*.

[20] Laurent C, Bauerheim M, Poinsot T et al. A novel modal expansion method for low-order modeling of thermoacoustic instabilities in complex geometries. *Combustion and Flame* 2019; 206: 206. DOI:10.1016/j.combustflame.2019.05.010.

[21] Silva CF, Nicoud F, Schuller T et al. Combining a helmholtz solver with the flame describing function to assess combustion instability in a premixed swirled combustor. *Combustion and Flame* 2013; 160: 1743–1754. DOI:10.1016/j.combustflame.2013.03.020.

[22] Gruber A, Bothien MR, Ciani A et al. Direct numerical simulation of hydrogen combustion at auto-ignitive conditions: Ignition, stability and turbulent reaction-front velocity. *Combustion and Flame* 2021; 229. DOI:10.1016/j.combustflame.2021.02.031.

[23] Casel M and Ghani A. Analysis of the flame dynamics in methane/hydrogen fuel blends at elevated pressures. *Proc Combust Inst* 2023; 39: 4631–4640. DOI:10.1016/j.proci.2022.07.211.

[24] Gruber A, Meyer OHH, Heggset T et al. Numerical investigation of reheat hydrogen flames in the sequential-combustion stage of a heavy-duty gas turbine. In *Proceedings of ASME Turbo Expo 2024 Turbomachinery Technical Conference and Exposition GT2024*.

[25] Crocco L. Aspects of combustion stability in liquid propellant rocket motors part i: Fundamentals. Low frequency instability with monopropellants. *Journal of the American Rocket Society* 1951; 21: 163–178. DOI:10.2514/8.4393.

[26] Zellhuber M, Bellucci V, Schuermans B et al. Modelling the impact of acoustic pressure waves on auto-ignition flame dynamics. In *Proceedings of the European Combustion Meeting 2011*.

[27] Schulz O and Noiray N. Autoignition flame dynamics in sequential combustors. *Combust Flame* 2018; 192. DOI:10.1016/j.combustflame.2018.01.046.

[28] Bothien M, Lauper D, Yang Y et al. Reconstruction and analysis of the acoustic transfer matrix of a reheat flame from large-eddy simulations. *J Eng Gas Turbines Power* 2019; 141: 021018. DOI:10.1115/1.4041151.

[29] Mcclure J, Berger FM, Bertsch M et al. Self-excited high-frequency transverse limit-cycle oscillations and associated flame dynamics in a gas turbine reheat combustor experiment. In *Proc. of ASME Turbo Expo 2021*.

[30] Gopalakrishnan HS, Heggset T, Gruber A et al. Prediction of autoignition-stabilized flame dynamics in a backward-facing step reheat combustor. In *Proc. of Combustion Institute-Canadian Section*.

[31] Gopalakrishnan HS, Gruber A and Moeck JP. Computation and prediction of intrinsic thermoacoustic oscillations associated with autoignition fronts. *Combustion and Flame* 2023; 254: 112844. DOI:10.1016/j.combustflame.2023.112844.

[32] Heinzmann S, Gopalakrishnan H, Wood B et al. Linear stability analysis of transversal thermoacoustic modes in reheat combustors. *Journal of Engineering for Gas Turbines and Power* 2025; : 1–19DOI:10.1115/1.4069453. URL https://doi.org/10.1115/1.4069453. https://asmedigitalcollection.asme.org/gasturbinespower/article-pdf/doi/10.1115/1.4069453/7530914/gtp-25-1285.pdf.

[33] McClure J, Berger FM, Bertsch M et al. Observation of reactive shear layer modulation associated with high-frequency transverse thermoacoustic oscillations in a gas turbine reheat combustor experiment. *International Journal of Spray and Combustion Dynamics* 2022; 14: 131–142. DOI:10.1177/17568277221088192.

[34] Gant F. Thermoacoustics of advanced reheat combustion systems. *Symposium on Thermoacoustics in Combustion: Industry meets Academia (SoTiC 2021)* 2021; DOI:10.3929/ethz-b-000523447.

[35] Romero Vega P, Berger FM, Hummel T et al. Numerical design of a novel reheat combustor experiment for the analysis of high-frequency flame dynamics. In *Proceedings of ASME Turbo Expo 2018*.

[36] Franke F, Bothien M and Sattelmayer T. Flame transfer function measurements of hydrogen-enriched reheat flames. *Combustion and Flame* 2025; 273: 113949. DOI: https://doi.org/10.1016/j.combustflame.2024.113949. URL https://www.sciencedirect.com/science/article/pii/S0010218024006588.

[37] Berger FM, Hummel T, Romero Vega P et al. A novel reheat combustor experiment for the analysis of high-frequency flame dynamics - concept and experimental validation. In *Proceedings of ASME Turbo Expo 2018 Turbomachinery Technical Conference and Exposition*.

[38] ANSYS. Ansys fluent user's guide, 2024. URL http://www.ansys.com.

[39] Kulkarni R. *Large Eddy Simulation of Autoignition in Turbulent Flows*. PhD Thesis, Technische Universität München, 2013.

[40] Kulkarni R, Bunkute B, Biagioli F et al. Large eddy simulation of alstom's reheat combustor using tabulated chemistry and stochastic fields-combustion model. DOI:10.1115/GT2014-26053.

[41] Brandt M. *Beschreibung der Selbstzündung in turbulenter Strömung unter Einbeziehung ternärer Mischvorgänge*. PhD Thesis, Technische Universität München, 2005. URL https://mediatum.ub.tum.de/601964.

[42] Smith GP, Golden DM, Frenklach M et al. Gri-mech 3.0. Online, 1999. URL http://www.me.berkeley.edu/gri_mech/.

[43] Curl RL. Dispersed phase mixing: I. theory and effects in simple reactors. *AIChE Journal* 1963; 9(2): 175–181.

[44] Hansinger M, Ge Y and Pfitzner M. Deep residual networks for flamelet/progress variable tabulation with application to a piloted flame with inhomogeneous inlet. *Combustion Science and Technology* 2022; 194(8): 1587–1613. DOI:10.1080/00102202.2020.1822826.

[45] *Large Eddy Simulation of Flame Response to Transverse Acoustic Excitation in a Model Reheat Combustor*, *Turbo Expo*, volume Volume 2: Combustion, Fuels and Emissions, Parts A and B, 2012. DOI:10.1115/GT2012-68317. URL https://doi.org/10.1115/GT2012-68317. https://asmedigitalcollection.asme.org/GT/proceedings-pdf/GT2012/44687/243/

4221667/243_1.pdf.

[46] McClure J, Bothien M and Sattelmayer T. High-frequency mode shape dependent flame-acoustic interactions in reheat flames. *Journal of Engineering for Gas Turbines and Power* 2023; 145. DOI:10.1115/1.4055531.